

Article

# Parametric Design and Optimization of the Profile of Autonomous Underwater Helicopter Based on NURBS

Xinyu An <sup>†</sup>, Ying Chen <sup>†</sup>  and Haocai Huang <sup>\*,†</sup> 

Ocean College, Zhejiang University, Zhoushan 316021, China; anxinyu@zju.edu.cn (X.A.); ychen@zju.edu.cn (Y.C.)

\* Correspondence: hchuang@zju.edu.cn

† These authors contributed equally to this work.

**Abstract:** Autonomous Underwater Helicopter (AUH) is a disk-shaped Autonomous Underwater Vehicle (AUV), and it has comparative advantage of near-bottom hovering and whole-direction turn-around ability over the traditional slender AUV. An optimization design of its irregular geometric profile is essential to improve its hydrodynamic performance. A parametric representation of its profile is proposed in this paper using Non-Uniform Rational B-spline (NURBS) curve. The parametric representation of AUH profile is described with two decision variables and several data points. Based on this parametric curve, Computational Fluid Dynamics (CFD) simulation is carried out to evaluate its hydrodynamic performance with various parameters. A predication model is established over variables' design space using Kriging surrogate model with CFD simulation results and a Genetic Algorithm (GA) procedure is conducted to find optimal design variables, which can produce an optimum lift-drag ratio. CFD verification results confirm that AUH profile with optimized design variables can increase its lift-drag ratio by 2.11 times compared with that of non-optimized ones. It demonstrates that the parametric representation and optimization procedure of AUH profile proposed in this paper is feasible, and it has a great potential in improving AUH's performance.

**Keywords:** Autonomous Underwater Helicopter (AUH); parametric design; Non-Uniform Rational B-spline (NURBS); Computational Fluid Dynamics (CFD)



**Citation:** An, X.; Chen Y.; Huang H. Parametric Design and Optimization of the Profile of Autonomous Underwater Helicopter Based on NURBS. *J. Mar. Sci. Eng.* **2021**, *9*, 668. <https://doi.org/10.3390/jmse9060668>

Academic Editor: Alessandro Ridolfi

Received: 7 May 2021  
Accepted: 11 June 2021  
Published: 16 June 2021

**Publisher's Note:** MDPI stays neutral with regard to jurisdictional claims in published maps and institutional affiliations.



**Copyright:** © 2021 by the authors. Licensee MDPI, Basel, Switzerland. This article is an open access article distributed under the terms and conditions of the Creative Commons Attribution (CC BY) license (<https://creativecommons.org/licenses/by/4.0/>).

## 1. Introduction

Autonomous Underwater Helicopter (AUH) is a novel disk-shaped, multi-propelled underwater vehicle, which is typically distinguished from traditional torpedo-shaped Autonomous Underwater Vehicle (AUV) in its configuration. This configuration makes it gain advantages in high mobility such as flexible steering, minimum radius of gyration and spot hovering. Since it was proposed by Professor Chen in 2017 [1], various research about its motion stability [2], control system [3], wave-entry impact force [4] and hydrodynamic resistance [5] has been conducted over the past few years. However, systematic design research on AUH's irregular geometric profile has not been carried out to the authors' knowledge. It is meaningful to design AUH's smooth profile curve to both satisfy its interior space requirement and improve its performance in hydrodynamics.

In practical engineering application, it is necessary to produce smooth and accurate geometric representation of engineering model for isogeometric analysis (IGA). Various methods were designed to represent the irregular profile of complex shapes with the use of computer aided design (CAD) methodologies and software tools. NACA airfoils were first and most widely used in the aircraft aerodynamic design and optimization at the very beginning. Class function/shape function transformation (CST) geometry representation method was then introduced and can be used to a universal three-dimensional geometry by means of describing the distribution of fundamental shapes [6]. Ciampa et al. combined CST parametrization and multidisciplinary design and optimization (MDO) to enhance the predesign stage for unconventional aircraft configuration [7] and this approach showed

good potentials for the predesign of blended wing body aircraft. Cai et al. adopted NACA airfoils as cross-section to design a soft body underwater vehicle called Robo-ray II [8]. Its motion deformation is conformable well with cow-nosed ray in nature, and it swims smoothly in water. Non-Uniform Rational B-spline (NURBS) is used to model real natural or artificial objects with a cloud of data points on their surface in most CAD software [9,10], especially in the geometric design of complex curves and surfaces such as aircraft, cars and ship hulls. Koini et al. presented a software tool for the conceptual design of turbomachinery bladings with 3D NURBS surfaces [11], and it can interactively construct parametric 3D blade of various types. Propeller blades, which are typically defined by a series of cross-sectional profiles placed along the radial locations, are now produced in B-spline representation [12]. Arapakopoulos et al. represented and compared marine propeller model further with NURBS and T-splines [13]. T-spline based parametric model was also used in a ship-hull representation and optimization process which can remove deficiencies due to the multi-patch NURBS representation of ship hull [14]. In this paper, NURBS curve is selected to represent AUH hull, whose shape profile is depicted with several data points and certain design parameters. The parametric representation of AUH's profile is the basis to improve its performance for follow-up research.

To form a NURBS curve, a common way is to shape the curve by several control points with variable parameters such as position, weight and knot vector. Optimization procedure is necessary to be performed to find optimal decision variables for these parametric NURBS curves. Various optimization methods have been designed and applied in practical engineering problems in order to balance economy and timeliness. Using those optimization methods and models, a relatively optimal result for design variables can be obtained based on data of limited sample points. Surrogate models such as polynomial response surfaces, Kriging, gradient-enhanced Kriging (GEK), radial basis function, support vector machine (SVM) and neural network (NN) are widely developed to establish a predication model for expensive "black-box" problem. Based on established predication model, multiple optimization algorithms such as Sequential Quadratic Programming (SQP), Genetic algorithm (GA), Simulated Annealing (SA) and Particle Swarm Optimization (PSO) can be employed to search for an optimal solution in given design space. This approach has been conducted to solve various engineering problems, both aerial and underwater. Genetic Algorithm was used in the real-time unmanned aerial vehicle path planning, which produced superior trajectories to the PSO [15]. Zhu et al. proposed a RBF surrogate model based on transfer learning to optimize aerodynamic performance of a low Reynolds number airfoil [16]. Steer et al. adopted artificial neural network (ANN) to design microwave circuits [17]. A neural network based method was implemented to construct the prediction interval of electrical power system's load forecasting and PSO was used to solve the problem [18]. The optimization procedure was also widely used to solve underwater engineering problems such as turbine blade optimization, hydrodynamic shape design of AUV, path planning and so on. Durali and Delnavaz developed a combined neural network and genetic algorithm scheme to find the optimum external geometric ratio of the submarine and obtained optimal values that stayed in minimum hydrodynamic forces [19]. Zou et al. presented a PSO based topology control mechanism for AUVs operating in unknown three-dimensional underwater spaces, which can guide AUVs in creating a protection area [20]. Lucas et al. composed a path simulator and genetic algorithm to help multi-objective glider path planning in real missions [21]. For the parametric AUH's NURBS curve presented in this paper, an optimization procedure combining Kriging surrogate model and genetic algorithm is adopted to optimize AUH hull in order to obtain its optimum hydrodynamic performance. This optimization procedure can provide a feasible way to optimize AUH's profile.

The parametric representation of AUH's profile is a worthwhile research, and it is essential to improve AUH's motion performance. This paper aims to construct a parametric representation of AUH's profile and improve its hydrodynamic performance, taking advantage of the existing feasible method. In this paper, a parametric NURBS curve with two

design variables is proposed to represent the AUH’s profile and the presented parametric curve is optimized to improve its hydrodynamic efficiency. This paper is organized as follows. First, AUH’s height is determined from aspects of hydrodynamic performance and interior payload space. The NURBS curve of AUH profile is parameterized with the angles at its two data points, which span a variable design space. Computational Fluid Dynamics (CFD) simulation is carried out to evaluate profile’s performance at certain sample points of design space. Then based on the simulation data obtained at sample points, a Kriging surrogate model is employed to establish a prediction model over the whole design space of decision variables. A GA optimization procedure is then performed to find the optimal angle pair, which corresponds to a maximum lift-drag ratio. Finally, the hydrodynamic performance of optimized AUH NURBS hull is simulated, which is proved to have a good improvement compared with that of the non-optimized one.

**2. Optimization Procedure of AUH Profile**

*2.1. NURBS Parameterization Method*

The AUH profile is depicted with NURBS curves, due to its generality in geometry design. NURBS is built from B-spline, and its control points have influence on local patches rather than entire domain, which makes it more flexible to represent general geometry [22]. The *k*-th degree NURBS curve is mathematically defined as:

$$C(u) = \sum_{i=0}^n R_{i,k}(u)P_i \tag{1}$$

where,  $\mathbf{U} = [a, a, \dots, a, u_{k+1}, u_{k+2}, \dots, u_{m-k-1}, b, b, \dots, b]$  is knot vector and  $m + 1$  is the number of its component.  $u$  is each component of  $\mathbf{U}$  and represents the parameter of spline curve’s piecewise function.  $R_{i,k}(u)$  is the rational basis function and  $k$  is its highest degree. The head and tail components of  $\mathbf{U}$  ( $a$  and  $b$ ) repeat for  $k + 1$  times to ensure generated curve pass corresponding control point.  $P_i$  represents the control points and  $n + 1$  is its number.  $R_{i,k}(u)$  can be expressed as:

$$R_{i,k}(u) = \frac{N_{i,k}(u)\omega_i}{\sum_{j=0}^n N_{j,k}(u)\omega_j} \tag{2}$$

$\omega_i$  is the weight of control point  $P_i$  and  $N_{i,k}(u)$  is the blending function defined on non-uniform control vector. It is expressed as:

$$N_{i,k}(u) = \frac{(u - u_i)N_{i,k-1}(u)}{u_{i+k} - u_i} + \frac{(u_{i+k} - u)N_{i+1,k-1}(u)}{u_{i+k} - u_{i+1}} \tag{3}$$

$$N_{i,k}(u) = \frac{(u - u_i)N_{i,k-1}(u)}{u_{i+k} - u_i} + \frac{(u_{i+k} - u)N_{i+1,k-1}(u)}{u_{i+k} - u_{i+1}} \tag{4}$$

$$N_{i,0}(u) = \begin{cases} 1, & u_i \leq u \leq u_{i+1} \\ 0, & else \end{cases}$$

*2.2. Genetic Algorithm*

Inspired by the evolutionist theory explaining the origin of species, the concept of GA was developed by Holland in the 1960s. GA is a population-based optimization method that is well suited for and widely used in the multi-objective optimization system of various practical problem for its high efficiency and convenience. The selection, crossover and mutation are the main operators of a GA process, which mimic the inheritance, random changes of genes in nature [23]. GA is more effective at performing global than traditional approaches, which compares the values of nearby points and moves the relative optimal points to perform local search. The general procedure of GA is shown in Figure 1.

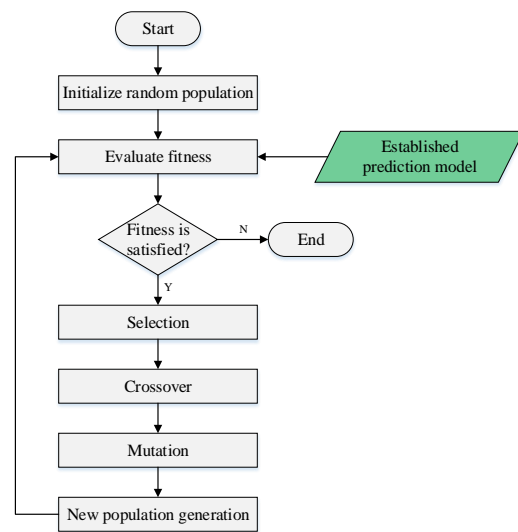


Figure 1. The general procedure of GA optimization method.

The fitness value, which is associated with the value of objective function of optimization problem, is evaluated against the unknown environment for each individual in the population in every generation. The fitness of each individual in every population can be evaluated with different approaches or predication models. In this paper, a Kriging surrogate model over the solution space of objective variable is established based on the results obtained from CFD simulation, which is conducted on predefined decision variable sample points. The GA optimization procedure is performed on the established predication model of objective variable, and corresponding decision variables for the optimal objective function are searched according to this evaluation approach.

2.3. Objective Function

In order to measure the hydrodynamic performance of designed AUH’s profile, the dimensionless presentations of the local static pressure, lift and drag force are used and these terms are obtained through the following expressions:

$$C_p = \frac{p - p_\infty}{\frac{1}{2}\rho U_\infty^2}, \quad C_L = \frac{F_L}{\frac{1}{2}\rho U_\infty^2 A}, \quad C_D = \frac{F_D}{\frac{1}{2}\rho U_\infty^2 A} \tag{5}$$

where,  $C_p$  is the pressure coefficient,  $p$  is the static pressure,  $p_\infty$  is the static pressure of the infinite flow,  $U_\infty$  is the inlet velocity,  $A$  is the projected area and  $F_L$  and  $F_D$  is lift and drag force around the AUH hull respectively.

Based on AUH’s parametric NURBS curve, this paper optimizes some design parameters to improve AUH’s hydrodynamic performance. The objective function for the optimization process can be expressed as:

$$f_{obj} = \min(-C_L/C_D) \tag{6}$$

where  $C_L$  is the lift coefficient of the curve, and  $C_D$  is its drag coefficient.

3. The Parametric NURBS Representation of AUH’s Profile

3.1. The Determination of AUH’s Height

The AUH’s profile is initiated as a disk-shaped rotating body, and its diameter and height are two important geometric parameters. According to practical application requirement, the radius of designed AUH is set to 530 mm, and its height needs to be determined on the basis of both payload capacity requirement and hydrodynamic efficiency. Hence, in the first step, the height-diameter ratio  $r = b/a$  of AUH should be determined. It is notable that  $a$  and  $b$  is half AUH’s diameter  $D$  and height  $H$ , respectively, i.e.,  $a = D/2$

and  $b = H/2$ . In order to investigate the effect of height-diameter ratio on AUH’s hydrodynamic performance, the profile of AUH’s hull is assumed as elliptic for simplicity in this section. AUH’s diameter is 1060 mm, and the determination of AUH’s height is processed on this basis. A series of different  $r$  values from 0.2 to 0.8 in a spacing of 0.2 are selected and studied to find a suitable value. The simplified AUH hull with different  $r$ s is illustrated in Figure 2.

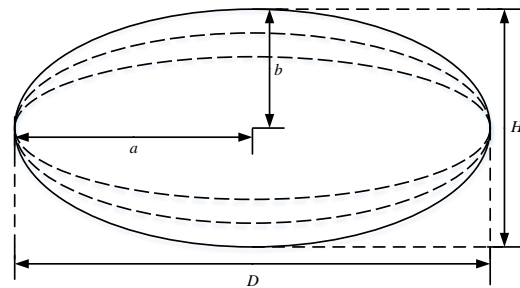


Figure 2. The schematic diagram of simplified AUH’s profile used for its height determination.

### 3.2. AUH Profile’s Parametric NURBS Representation

On the basis of designed AUH’s height-diameter ratio, the design of AUH’s overall profile curve will be carried out. Due to the AUH’s disk shape design, its contour is treated as bilateral symmetry both left-right and up-down. Therefore, the research is expanded on only a quarter of its outline. The AUH’s profile is depicted by a NURBS curve defined with two fixed data points, i.e., the horizontal vertex **A** and vertical vertex **B**. Two additional shape points **C** and **D** are appended, whose spatial positions are determined by the inner mechanical construction requirement—a pressure chamber and horizontal propellers separately. With selected diameter and height values, the coordinates of shape points **C** and **D** are determined. Thus the AUH’s parametric NURBS profile is sketched with four data points and its slopes at two data points, which is illustrated in Figure 3a. The curve’s slope is infinite at the shape point **A** and zero at the shape point **B**. Finally, the curve’s shape is controlled by two slopes at its data points **C** and **D**, which are depicted by two angles of inclination  $\theta_C$  and  $\theta_D$ . The parametric AUH’s outline is illustratively shown in Figure 3b. This parametric NURBS curve is used for the follow-up optimization design of AUH’s profile.

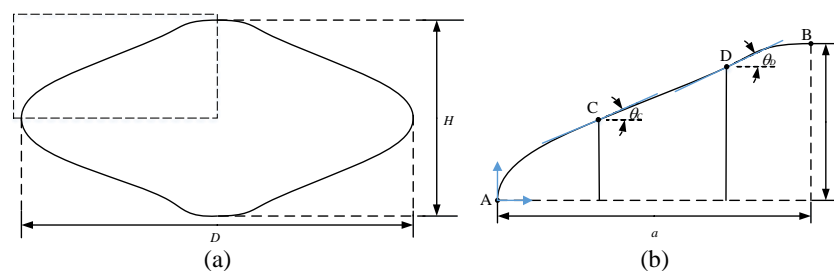


Figure 3. The sketch of AUH’s NURBS profile and its parametric description: (a) the overall outline, (b) a quarter profile with parametric variables.

### 3.3. Parametric Variable Setups of AUH Profile

Based on the proposed parametric NURBS representation of AUH’s curve, two slant angles  $\theta_C$  and  $\theta_D$  at data points **C** and **D** shape AUH’s profile. Hence, the degrees of these two angles are selected as decision variables and a optimization procedure will be conducted on their design space to improve AUH’s overall performance. In this paper, CFD simulation and GA approach is performed sequentially to optimize these angles of inclination.

#### 4. CFD Simulation Setups and Validation

The hydrodynamic performance of different AUH profiles is evaluated with CFD approach. According to the evaluation of its performance at several sample points in decision variables’ design space, a predication model is generated over stated design space, which can be used for the following optimization procedure. The setups for CFD simulation are introduced in the following.

##### 4.1. Computational Domain and Boundary Conditions

An adequate computational zone with a width of  $20H$  and a length of  $40D$  is adopted in order to achieve accurate simulation results [24], as shown in Figure 4. The AUH’s profile model is vertically centered and horizontally located  $15D$  from the inlet wall, thus a  $25D$ -long zone remains to ensure the complete development of turbulent flow in AUH’s wake. In the neighborhood of placed model, a zone of  $5D$  along flow and  $4H$  across flow is refined with grids of smaller size to acquire accurate result. Near the model, boundary layers are adopted to capture the near-wall flow.

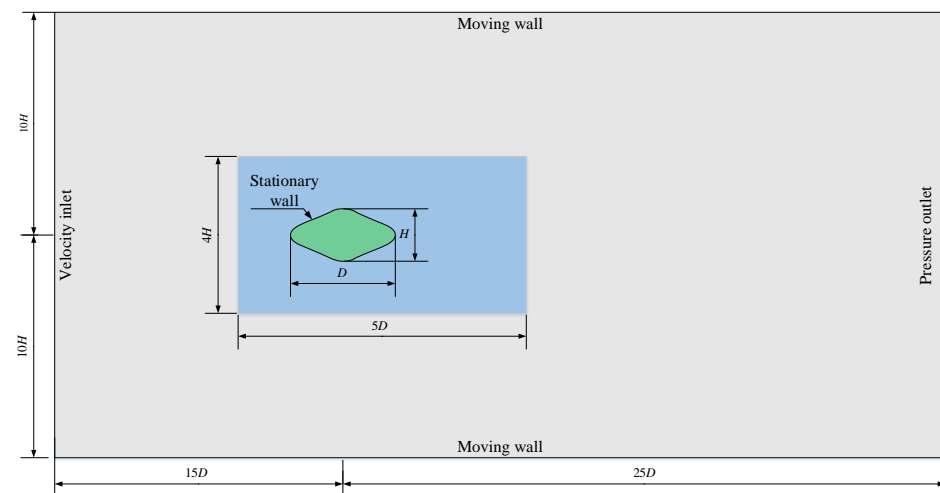


Figure 4. The computational domain and boundary conditions used for CFD simulation.

The left wall is set as velocity inlet with a fixed horizontal velocity value, and the right wall is set as pressure outlet. The top and bottom is set as moving walls with the same value of inlet velocity due to the wide computational zone adopted in this paper. The AUH model edge is set as stationary wall.

##### 4.2. CFD Governing Equation

The CFD simulation is carried out using commercial code Fluent 19.0, which is based on finite volume method. Since AUH works in underwater environment, the governing equations are Navier–Stokes equations for the incompressible viscous flow including the mass and momentum conversations in unsteady forms and they are written as:

$$\nabla \cdot \mathbf{U} = 0$$

$$\frac{\partial \mathbf{U}}{\partial t} + (\mathbf{U} \cdot \nabla) \mathbf{U} = -\frac{1}{\rho} \nabla p + \nu \nabla^2 \mathbf{U} \tag{7}$$

where,  $\mathbf{U}$  is the velocity vector,  $\rho$  is fluid’s density,  $p$  is the fluid pressure and  $\nu$  is fluid’s kinematic viscous.

The Reynolds averaged method is adopted in solving Equation (7), which corresponds to the Reynolds Averaged Navier–Stokes (RANS) equations. The term of Reynolds stresses is brought in, and turbulence models need to be introduced to closure RANS equations. The SST (Shear Stress Transport)  $k-\omega$  model, which is a hybrid model combing  $k-\omega$  and  $k-\epsilon$

model, has better performance in capturing boundary layer flow and is employed in the CFD simulation of this paper.

4.3. CFD Method Verification and Validation

The hydrodynamic performance of AUH model is evaluated to verify the CFD simulation method. According to AUH’s motion stability in underwater environment, its traveling speed is set to 1 m/s. Thus the simulation is performed under  $Re = \frac{U_{\infty}D}{\nu} = 1.06 \times 10^6$ . In order to validate the method and mesh used in simulation more effectively, a circular model is adopted in this step.

The entire computational domain is discretized with quadrilateral elements and the domain around the AUH model is refined with small mesh size. Second-order upwind scheme is the mostly widely used discretization scheme because of its stability, and it gives good results for most classes of flows. Hence, a second-order upwind spatial discretization scheme is used for all fluid-governing equations, including pressure, momentum and turbulence. The criteria of all scaled residuals including continuity equation, momentum equation,  $k$  equation and  $\omega$  equation below  $1 \times 10^{-5}$  are employed as the convergence criterion in order to get reliable results. The timestep is set as 0.001 s and the maximal iteration of each time step are set to 30, which enables all residuals to reach convergence in every time step.

Mesh verification is carried out on three different mesh precision, and simulation results are listed in Table 1. Since fluid field variation occurs more rapidly near the AUH model, only the mesh precision in the refined zone is modified to change the overall element number, which means the total element number is mainly influenced by that of the refined zone.

Table 1. Mesh verification for different mesh size.

Mesh Type	Cell Number	Refined Zone Element Size	$C_D$
Coarse	288713	40	0.3050
Medium	356313	20	0.3167
Fine	978743	10	0.3265
LES [25]	–	–	0.31
Experimental results [26,27]	–	–	0.17–0.40

Table 1 reveals that  $C_D$ s obtained from three mesh types in this simulation have some deviations from that of LES and  $C_D$  of the fine case is slightly larger than that of other two cases. This deviation mainly derives from Reynolds averaged method adopted in solving governing NS equations. However, drag coefficients are all within reasonable limits compared with others’ experimental results. From the coarse case to medium one, cell number increases by 23.41%, while from the medium case to the fine one this value is 174.69%, which means an obvious increase in computation costs. Therefore, the element size of refine zone around AUH model in the following simulation cases is set as 20 mm, which can provide credible results and reduces computation cost at the same time.

5. Results and Analysis

5.1. AUH’s Height and Data Points

CFD simulation process mainly consists of two parts: the determination of AUH’s height and the simulation on decision variables’ predefined sample points. AUH’s height-diameter ratio is identified first based on a simplified elliptic model. Then the data points of parametric NURBS curve are acquired and CFD simulation is carried out based on this parametric NURBS curve.

A series of CFD simulations on the simplified AUH model with different height-diameter ratios is performed, and corresponding hydrodynamic coefficients are achieved. The variations of lift, drag coefficients and their ratio under chosen height-diameter ratios are plotted in Figure 5.

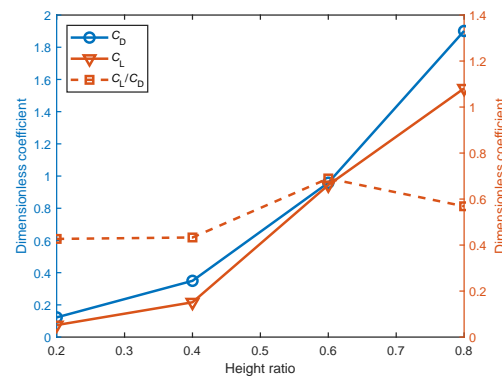


**Figure 5.** The variation of lift coefficient, drag coefficient and their ratio around AUH’s model versus its height-diameter ratio.

It is observed in Figure 5 that drag coefficient is generally greater than the lift one for simulation cases. Drag coefficient barely raises monotonously with the increase of  $r$ , and drag force should be restricted to improve AUH’s propulsive efficiency. Taken the limit of lift coefficient at  $r = 0.2$  and the drag coefficient at  $r = 0.8$  into consideration, an appropriate height-diameter ratio of 0.4 is selected in simulated cases. According to above simulation results and the interior space requirement, AUH’s height is set as 416 mm, and its specified height-diameter ratio is 0.393. Therefore, the basic dimensions of AUH are listed in Table 2.

**Table 2.** AUH’s basic dimensions used for following simulation cases.

Diameter/mm	Height/mm	$r$
1060	416	0.393

As shown in Figure 3b, the parametric NURBS curve is defined with four data points and two angles of inclination. With AUH’s height-diameter ratio selected above and the dimensions of its inner equipment, the coordinates of these data points are determined and they are listed in Table 3.

**Table 3.** Data points definition for the parametric NURBS curve to be optimized.

Data Point	A	B	C	D
$x$ -coordinate	0	$a$	$0.332a$	$0.774a$
$y$ -coordinate	0	$b$	$0.625b$	$0.913b$

Both degrees of these two decision angles are confined to its adjacent shape points, i.e., **A** and **B**, to avoid AUH curve’s obvious distortion. Therefore, for sample points in the design space, the degree of decision variables  $\theta_C$  and  $\theta_D$  ranges from  $5^\circ$  to  $37^\circ$  in a spacing of  $8^\circ$  and from  $8^\circ$  to  $28^\circ$  in an interval of  $5^\circ$  separately in the following simulation.

### 5.2. Evaluation of Hydrodynamic Performance

The hydrodynamic performance of AUH hull shaped with different  $\theta_C$  and  $\theta_D$  is evaluated sequentially. Its performance on drag coefficient, lift coefficient and lift-drag ratio is analyzed separately.

#### 5.2.1. Drag Coefficient

AUH’s drag, which is a key factor to reduce AUH’s energy consumption, is greatly influenced by its profile. For the simulation cases, the variation of AUH’s drag coefficient versus design parameters  $\theta_C$  and  $\theta_D$  is presented in Figure 6.

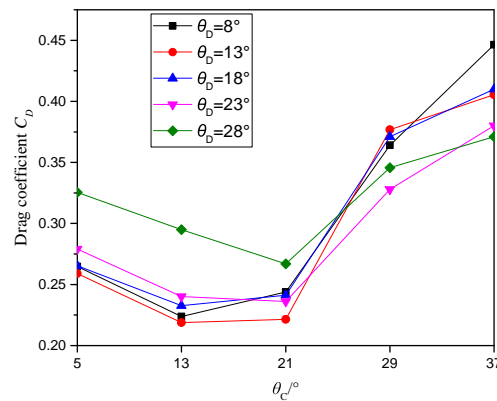


Figure 6. Variation of drag coefficient around AUH versus different design parameters  $\theta_C$  and  $\theta_D$ .

It can be found in Figure 6 that drag coefficient  $C_D$  decreases with the increase of  $\theta_C$  when this angle is smaller than a certain angle around  $21^\circ$ . It increases dispersedly with various  $\theta_D$ s when  $\theta_C$  is greater than that angle. The same trend is observed for every  $\theta_D$  series, and it can be more clearly illustrated for a series with the same  $\theta_D$ , such as  $\theta_D = 13^\circ$  shown in Figure 7. With a smaller  $\theta_C$  (as  $5^\circ$  shown in Figure 7a), a more rounded leading corner at AUH’s front is formed, which produces a low pressure area near the design point C at the leading edge. The same situation occurs near the design point D with a greater  $\theta_C$  (as  $29^\circ$  shown in Figure 7d). This additional induced low pressure area increases AUH’s drag significantly, and it almost completely dissipates at  $\theta_C = 13^\circ$  and  $21^\circ$  (as shown in Figure 7b,c). Therefore, V-shaped variation trend of drag coefficient for a series of  $\theta_D$  is induced by varying low pressure area. The descent at left side is controlled by that near the design point C, while the ascent at its right side is controlled by that near the design point D.

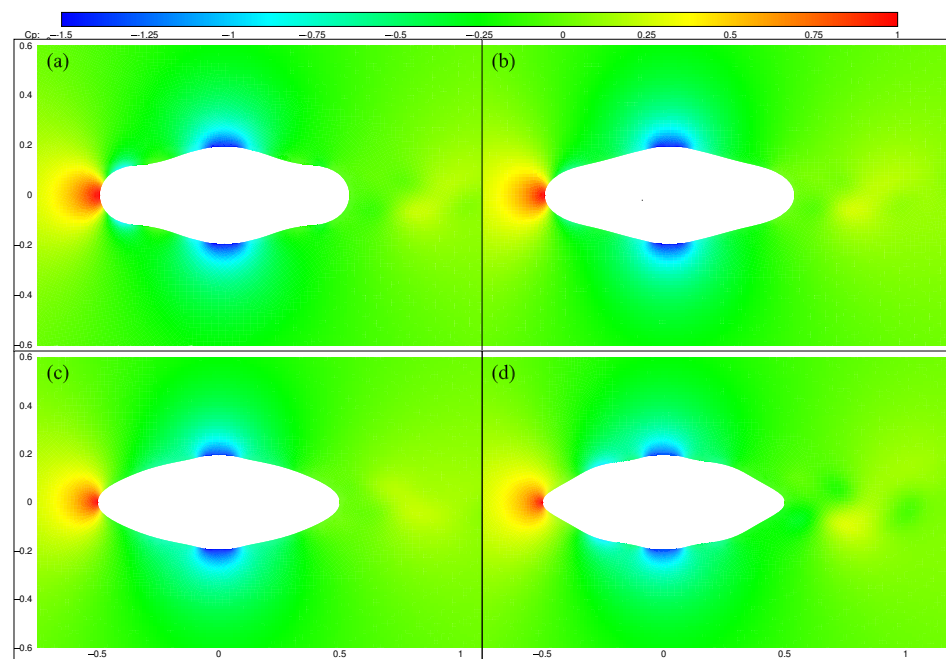
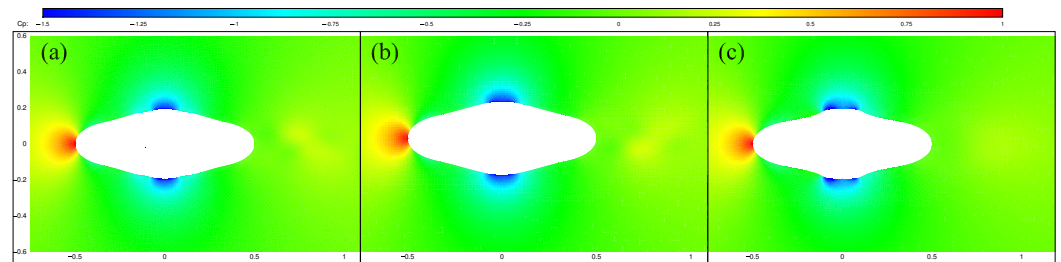


Figure 7. The contour of pressure coefficient around AUH model for different simulation cases of  $\theta_D = 13^\circ$ : (a)  $\theta_C = 5^\circ$ ; (b)  $\theta_C = 13^\circ$ ; (c)  $\theta_C = 21^\circ$ ; (d)  $\theta_C = 29^\circ$ . (Both  $x$  and  $y$  coordinate is nondimensionalized with AUH’s diameter  $D$ ).

Besides, when  $\theta_C$  is less than  $21^\circ$ ,  $C_D$ s at  $\theta_C = 13^\circ$  are generally smaller than those at  $5^\circ$ . This results from the fact that small  $\theta_D$  induces a subtle local hump and slight pressure drop near design point D and curving segment DB, as shown in Figure 8a,b.  $C_D$  tends to

increase consistently with  $\theta_D$  for the same  $\theta_C$  when  $\theta_C$  is less than  $13^\circ$ . This is due to the fact that bigger  $\theta_C$  smooths the curve between **C** and **D**, and causes a broader and flatter area near AUH's top. Then two relatively independent low pressure areas are formed, and one in the upwind side is distinctly stronger than the other one in the downwind side, as shown in Figure 8c. An opposite trend is found for the serial simulation cases of  $\theta_C = 37^\circ$ . When  $\theta_C$  is large enough, low pressure area near point **C** has a greater influence. The bigger the difference between  $\theta_C$  and  $\theta_D$  is, the more clear the formed hump is and therefore lower pressure near point **C** is induced. Thus drag coefficient at  $\theta_D = 8^\circ$  is maximal in this simulation series.



**Figure 8.** The contour of pressure coefficient around AUH model for different simulation cases of  $\theta_C = 13^\circ$ : (a)  $\theta_D = 8^\circ$ ; (b)  $\theta_D = 13^\circ$ ; (c)  $\theta_D = 28^\circ$ . (Both  $x$  and  $y$  coordinate is nondimensionalized with AUH's diameter  $D$ ).

### 5.2.2. Lift Coefficient

The lift coefficient on different AUH hulls is measured by the root mean square (RMS) value of the undulatory lift force. In order to estimate the influence of selected decision variables on  $C_L$  over the entire design space, the variation of AUH's lift coefficient in different simulation cases is shown in Figure 9.

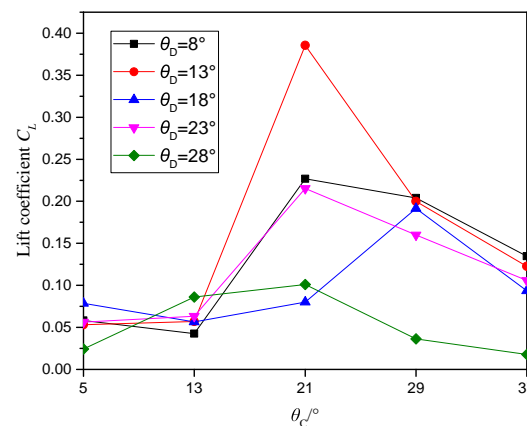


**Figure 9.** Variation of lift coefficient around AUH model versus different design parameters  $\theta_C$  and  $\theta_D$ .

It can be found in Figure 9 that for a series of simulation cases with the same  $\theta_D$ , lift coefficient experiences a similar variation trend. It raises first and then drops with the increase of  $\theta_C$  and maximum lift coefficient is obtained under  $\theta_D$  in an interval of  $[21^\circ, 29^\circ]$ . The lift variation among those simulated cases can be explained by the pressure distribution around the AUH's hull and six typical pressure distribution are shown in Figure 10.

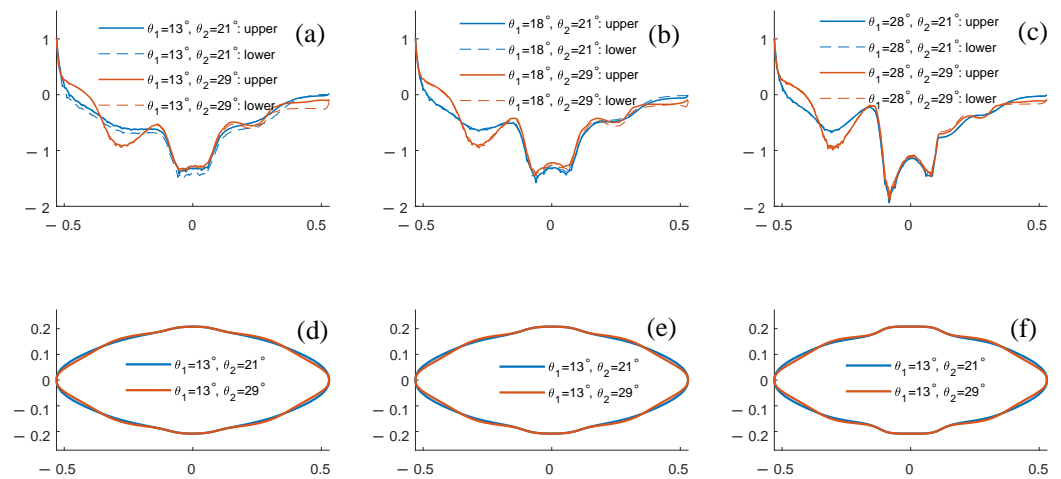


**Figure 10.** The comparison of pressure distribution around AUH’s hull and corresponding AUH contours with different parameters: pressure distribution around AUH’s upper and lower for (a)  $\theta_C = 13^\circ, \theta_D = 21^\circ$  and  $\theta_C = 13^\circ, \theta_D = 29^\circ$ ; (b)  $\theta_C = 18^\circ, \theta_D = 21^\circ$  and  $\theta_C = 18^\circ, \theta_D = 29^\circ$ ; (c)  $\theta_C = 28^\circ, \theta_D = 21^\circ$  and  $\theta_C = 28^\circ, \theta_D = 29^\circ$ ; (d–f): corresponding AUH’s hull respectively.

It can be seen from Figure 10 that a great pressure difference exists between AUH’s upper and lower surface, which produces a relatively large lift force at  $\theta_C = 13^\circ, \theta_D = 21^\circ$  compared with other cases. The change of slant angles  $\theta_C$  and  $\theta_D$  affects pressure distribution curve around AUH’s surface through the same mechanism. For a certain pair of  $\theta_C$  and  $\theta_D$ , the parametric NURBS curve will form a concave or convex section between local zone in curve sections AC, CD and DB as shown in Figure 3b and Figure 10b. At the concave section, fluid flow is blocked, which produces a local speed drop and thereafter a pressure raise. While at the convex section, fluid flow is accelerated and a local pressure drop is induced. These local variations not only raise drag force significantly but also impel the pressure distribution at the upper and lower surface to be more consistent, which leads to the reduction of lift force.

### 5.2.3. Lift-Drag Ratio and Kriging Surrogate Model

The lift-drag ratio, which is the objective variable of this optimization problem, is obtained through dividing lift coefficient by corresponding drag coefficient. The variation of lift-drag ratio for simulated cases is shown in Figure 11a. It can be noticed that Figure 11a has similar variation trends with that of Figure 9, which results from the fact that the variation of  $C_D$  is relatively smaller than that of  $C_L$ .

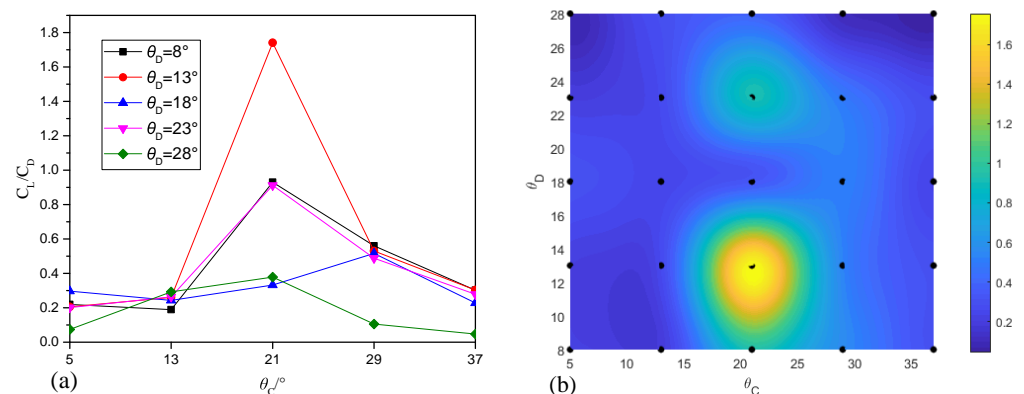


**Figure 11.** The lift-drag ratio: (a) variation with different simulation cases; (b) Kriging response surface model.

In order to search for the optimal design parameters, a prediction model over predefined design space of decision variables is obtained by means of Kriging surrogate model. The response surface model (RSM) of established prediction model for lift-drag ratio is presented in Figure 11b. It can be observed in Figure 11 that maximum lift-drag ratio is generally large in the neighborhood of  $(\theta_C, \theta_D) = (21^\circ, 13^\circ)$ .

5.3. GA Optimization Procedure and Verification

5.3.1. GA Optimization

A GA optimization procedure is carried out on the established Kriging prediction model of lift-drag ratio to search for optimal decision variables pair. The size of population for GA optimization is set to 150 and maximum generation is 100. The probability of crossover and mutation between each generation is both 0.4. Optimization results show that optimal design parameter is  $(21.14^\circ, 12.55^\circ)$ , where maximum lift-drag ratio is reached in predetermined optimization space. A verification process is followed to test the obtained results subsequently.

5.3.2. Verification of Optimization Result

The optimized AUH profile generated with obtained decision variables is shown in Figure 12a. Figure 12a illustrates that the profile is smooth and no obvious distortion or hump/sinking exists over the whole curve. Based on optimization results, therewith corresponding three-dimensional AUH shell is displayed in Figure 12b. A CFD simulation procedure is carried out with this new hull to evaluate its hydrodynamic performance and then it is compared with that of others.

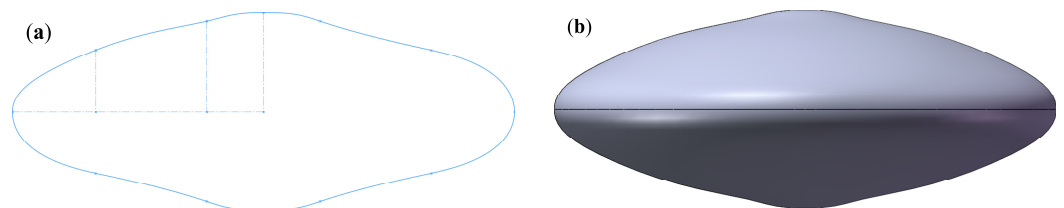


Figure 12. Optimization results: (a) AUH profile with optimized decision variables; (b) 3D AUH shell with optimal design parameters.

The flow field comparison around AUH model with optimized profile and non-optimized elliptic one (height-diameter ratio to be 0.393), in term of pressure coefficient distribution, is presented in Figure 13.

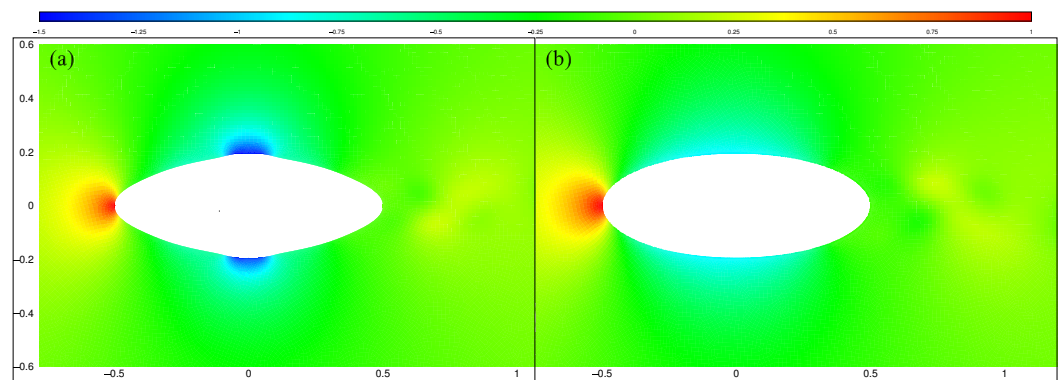


Figure 13. Snapshot of pressure contour around AUH with (a) optimized profile; (b) non-optimized elliptic curve. (Both  $x$  and  $y$  coordinate is nodimensionalized with AUH’s diameter  $D$ ).

Figure 13 reveals that the low pressure zone attached to non-optimized AUH's lower and upper surfaces is larger, while its amplitude is substantially smaller than that of the optimized one. The larger low pressure amplitude and flow separation boosts the lift force and the smaller low pressure area in the leading edge decreases the drag force, which together prompts AUH's hydrodynamic performance with the optimized profile.

Compared with the original AUH hull with a height-diameter ratio of 0.393, the final profile with optimized decision variables improves its lift coefficient by 129.97% and reduces its drag coefficient by 25.97%, thus its lift-drag ratio is 3.11 times the original one. The CFD verification results demonstrate that the proposed approach can improve AUH's hydrodynamic performance remarkably by optimizing certain parameters.

## 6. Conclusions

A parametric representation and an optimization approach of AUH's profile is proposed in this paper. Firstly, AUH's irregular profile is represented using a NURBS curve with four data points, which is parameterized with two design variables:  $\theta_C$  and  $\theta_D$ . Then, a series of CFD simulations is conducted over the design space, and a Kriging response surface prediction model of AUH's lift-drag ratio is established over the whole space. Finally, a GA optimization procedure is carried out based on established prediction model to search for optimal decision variables. CFD verification demonstrates that the optimized AUH profile can improve its hydrodynamic performance significantly. The main conclusions of this paper are summarized as follows:

- A parametric representation of AUH profile is present using NURBS curve with four data points and two decision angles. This NURBS representation can be further used to design and optimize AUH's shape geometry and other concerned geometric parameters.
- In the NURBS representation curve, the change of parametric parameters generally affects the shape of a curve section near the control point. Varying decision angles can result in a local concave/convex section around corresponding data point, which is the main reason to cause local pressure fluctuation and increase its drag.
- With the parametric representation and optimization approach of AUH profile proposed in this paper, the optimized AUH profile can improve its lift-drag ratio by 210.63% compared with that of the non-optimized elliptic one.

Based on this optimized AUH profile, a systemic research about its motion stability and manoeuvrability based on this AUH model with multi-propellers and payload sensors is ongoing. Corresponding prototype is also being designed and manufactured.

**Author Contributions:** Conceptualization, Y.C., H.H. and X.A.; methodology, H.H. and X.A.; validation, X.A.; formal analysis, H.H. and X.A.; investigation, H.H. and X.A.; resources, Y.C., H.H. and X.A.; data curation, X.A.; writing—original draft preparation, X.A.; writing—review and editing, H.H. and Y.C.; visualization, X.A. and H.H.; supervision, Y.C. and H.H.; project administration, Y.C. and H.H.; funding acquisition, Y.C., H.H. and X.A. All authors have read and agreed to the published version of the manuscript.

**Funding:** This work was supported by the National Key R&D Program of China (Grant No. 2017YFC0306100), the National Natural Science Foundation of China (Grant No. 52001279) and the Zhejiang Provincial Postdoctoral Science Foundation (Grant No. ZJ2020137).

**Conflicts of Interest:** The authors declare no conflict of interest.

## Abbreviations

The following abbreviations are used in this manuscript:

AUH	Autonomous Underwater Helicopter
AUV	Autonomous Underwater Vehicle
NURBS	Non-Uniform Rational B-spline
CFD	Computational Fluid Dynamics
SST	Shear Stress Transport
URANS	unsteady Reynold-averaged Navier–Stokes
LES	Large Eddy Simulation

## References

- Ji, D.; Chen, C.W.; Chen, Y. Autonomous Underwater Helicopters AUV with Disc-Shaped Design for Deepwater Agility. *Sea Technol.* **2018**, *59*, 25–27.
- Chen, C.W.; Jiang, Y.; Huang, H.C.; Ji, D.X.; Sun, G.Q.; Yu, Z.; Chen, Y. Computational fluid dynamics study of the motion stability of an autonomous underwater helicopter. *Ocean Eng.* **2017**, *143*, 227–239. [[CrossRef](#)]
- Liu, X.; Wang, Z.; Guo, Y.; Wu, Y.; Wu, G.; Xu, J.; Chen, Y. The design of control system based on autonomous underwater helicopter. In Proceedings of the OCEANS 2018 MTS/IEEE Charleston, Charleston, SC, USA, 22–25 October 2018. [[CrossRef](#)]
- Chen, C.W.; Wang, T.; Feng, Z.; Lu, Y.; Huang, H.; Ji, D.; Chen, Y. Simulation research on water-entry impact force of an autonomous underwater helicopter. *J. Mar. Sci. Technol.* **2020**, *25*, 1166–1181. [[CrossRef](#)]
- Lin, Y.; Huang, Y.; Zhu, H.; Huang, H.; Chen, Y. Simulation study on the hydrodynamic resistance and stability of a disk-shaped autonomous underwater helicopter. *Ocean Eng.* **2021**, *219*. [[CrossRef](#)]
- Kulfan, B.M. Universal Parametric Geometry Representation Method. *J. Aircr.* **2008**, *45*, 142–158. [[CrossRef](#)]
- Ciampa, P.D.; Zill, T.; Nagel, B.; German, D.; Center, A. CST Parametrization for Unconventional Aircraft Design Optimization. In Proceedings of the Congress of the International Council of the Aerospace Sciences, Nice, France, 19–24 September 2010.
- Cai, Y.; Bi, S.; Zheng, L. Design and Experiments of a Robotic Fish Imitating Cow-Nosed Ray. *J. Bionic Eng.* **2010**, *7*, 120–126. [[CrossRef](#)]
- Dimas, E.; Briassoulis, D. 3D geometric modelling based on NURBS: A review. *Adv. Eng. Softw.* **1999**, *30*, 741–751. [[CrossRef](#)]
- Hughes, T.J.R.; Cottrell, J.A.; Bazilevs, Y. Isogeometric analysis: CAD, finite elements, NURBS, exact geometry and mesh refinement. *Comput. Methods Appl. Mech. Eng.* **2005**, *194*, 4135–4195. [[CrossRef](#)]
- Koini, G.N.; Sarakinos, S.S.; Nikolos, I.K. A software tool for parametric design of turbomachinery blades. *Adv. Eng. Softw.* **2009**, *40*, 41–51. [[CrossRef](#)]
- Pérez-Arribas, F.; Pérez-Fernández, R. A B-spline design model for propeller blades. *Adv. Eng. Softw.* **2018**, *118*, 35–44. [[CrossRef](#)]
- Arapakopoulos, A.; Polichshuk, R.; Segizbayev, Z.; Ospanov, S.; Ginnis, A.; Kostas, K. Parametric models for marine propellers. *Ocean Eng.* **2019**, *192*, 106595. [[CrossRef](#)]
- Kostas, K.; Ginnis, A.; Politis, C.; Kaklis, P. Ship-hull shape optimization with a T-spline based BEM–isogeometric solver. *Comput. Methods Appl. Mech. Eng.* **2015**, *284*, 611–622. [[CrossRef](#)]
- Roberge, V.; Tarbouchi, M.; Labonte, G. Comparison of Parallel Genetic Algorithm and Particle Swarm Optimization for Real-Time UAV Path Planning. *IEEE Trans. Ind. Inform.* **2013**, *9*, 132–141. [[CrossRef](#)]
- Zhu, Z.; Guo, H. Design of an RBF Surrogate Model for Low Reynolds Number Airfoil Based on Transfer Learning. In Proceedings of the 2019 Chinese Control and Decision Conference (CCDC), Nanchang, China, 3–5 June 2019; pp. 4555–4559. [[CrossRef](#)]
- Steer, M.B.; Bandler, J.W.; Snowden, C.M. Computer-aided design of RF and microwave circuits and systems. *IEEE Trans. Microw. Theory Tech.* **2002**, *50*, 996–1005. [[CrossRef](#)]
- Quan, H.; Srinivasan, D.; Khosravi, A. Short-Term Load and Wind Power Forecasting Using Neural Network-Based Prediction Intervals. *IEEE Trans. Neural Netw. Learn. Syst.* **2014**, *25*, 303–315. [[CrossRef](#)] [[PubMed](#)]
- Durali, M.; Delnavaz, A. BEM/FEM simulation of acoustic field and shape optimization of submarine using neural network and genetic algorithm. In Proceedings of the 2004 International Symposium on Underwater Technology (IEEE Cat. No.04EX869), Taipei, Taiwan, 20–23 April 2004; pp. 283–287. [[CrossRef](#)]
- Zou, J.; Gundry, S.; Kusyk, J.; Sahin, C.S.; Uyar, M.Ü. Bio-inspired topology control mechanism for autonomous underwater vehicles used in maritime surveillance. In Proceedings of the 2013 IEEE International Conference on Technologies for Homeland Security (HST), Waltham, MA, USA, 12–14 November 2013; pp. 201–206. [[CrossRef](#)]
- Lucas, C.; Hernandez-Sosa, D.; Caldeira, R. Multi-Objective Four-Dimensional Glider Path Planning using NSGA-II. In Proceedings of the 2018 IEEE/OES Autonomous Underwater Vehicle Workshop (AUV), Porto, Portugal, 6–9 November 2018; pp. 1–5. [[CrossRef](#)]
- Nandi, A.; Siddavatam, R. On NURBS algorithms and application: A survey. In Proceedings of the 2015 2nd IEEE International Conference on Computing for Sustainable Global Development (INDIACom), New Delhi, India, 11–13 March 2015; pp. 2019–2024.
- Konak, A.; Coit, D.W.; Smith, A.E. Multi-objective optimization using genetic algorithms: A tutorial. *Reliab. Eng. Syst. Saf.* **2006**, *91*, 992–1007. [[CrossRef](#)]

24. Singh, Y.; Bhattacharyya, S.; Idichandy, V. CFD approach to steady state analysis of an underwater glider. In Proceedings of the 2014 Oceans-St. John's, St. John's, NL, Canada, 14–19 September 2014; pp. 1–5.
25. Vu, H.C.; Ahn, J.; Hwang, J.H. Numerical investigation of flow around circular cylinder with splitter plate. *KSCE J. Civ. Eng.* **2016**, *20*, 2559–2568. [[CrossRef](#)]
26. Zdravkovich, M.M. Conceptual overview of laminar and turbulent flows past smooth and rough circular cylinders. *J. Wind Eng. Ind. Aerodyn.* **1990**, *33*, 53–62. [[CrossRef](#)]
27. Lo, S.C.; Hoffmann, K.A.; Dietiker, J.F. Numerical investigation of high Reynolds number flows over square and circular cylinders. *J. Thermophys. Heat Transf.* **2005**, *19*, 72–80. [[CrossRef](#)]